Journal of Biomedical Optics 6(1), 74–85 (January 2001)

Temperature distributions in laser-heated biological tissue with application to birthmark removal

Michael K. Loze
C. David Wright
University of Exeter
School of Engineering and Computer Science
Exeter EX4 4QF
United Kingdom

Abstract. The time-dependent temperature distributions produced within thermally homogeneous media heated by a moving laser beam with Gaussian and uniform power density profiles are examined using a time-domain method based on Green's functions. Regions of finite length, width, and depth within the medium having exponential power absorption are considered. The temperature distribution is written as a single integral with respect to time of simple functions and the resulting expressions have been used to model the heating of blood vessels for birthmark (port-wine stain) removal. The temperature distributions obtained are in good agreement with those produced using Monte Carlo optical and finite difference thermal models. [DOI: 10.1117/1.1318217

Keywords: laser heating; temperature distribution; medical laser heating; port-wine stain removal.

Paper JBO-90051 received Sep. 20, 1999; revised manuscript received Aug. 18, 2000; accepted for publication Aug. 21, 2000.

1 Introduction

The heating effect of laser beams has found many applications in the medical field,[1,2] including eye and heart surgery and birthmark removal. Lasers are also used extensively in integrated circuit fabrication for annealing semiconductors[3] and optical recording systems for storing information in a multilayer recording medium.[4]

In this paper simple expressions for the three-dimensional (3D) time-dependent temperature distribution within a laser-heated medium containing arbitrarily shaped light-absorbing regions are derived. The thermal properties of the medium are assumed to be independent of temperature. Heat is produced in the medium by absorption of optical energy from an incident laser beam and diffuses through the medium in accordance with the linear heat conduction equation. The well-known Green's function method[5,6] is used to solve this heat conduction problem. Expressions for the temperature distributions within semi-infinite media have been examined perviously using this approach.[6–11] Temperature distributions in the absence of surface losses for laser angioplasty applications have also been examined in Ref. 7 while convective surface losses are included in Ref. 8. Surface precooling of the skin for port-wine stain (PWS) removal applications has been examined in detail in Refs. 9–11. In this paper the case of a finite-thickness medium is examined, resulting in much simplified mathematical forms that allow a wide range of heat generating rate cases to be solved. All spatial integrations are performed analytically so that the solutions require only one numerical integration (with respect to time) to be performed.

As an example of the application of the method presented, the heating of a blood vessel within the skin is examined. This situation arises in removal of birthmarks, such as PWS, where the laser is used to irreversibly damage the abnormal blood vessels causing the unwanted skin pigmentation.[2,12,13] In the literature the Green's function method has also been applied to the analysis of pulsed photothermal radiometry (PPTR)[14–16] and infrared tomography (IRT)[17,18] signals in order to examine the temperature distribution within PWS skin following laser irradiation. For analysis of PPTR signals the 1D linear heat conduction equation is assumed to apply within the skin. An inverse problem is then derived which can be solved to give the temperature increase after laser irradiation. The Green's function for a semi-infinite, thermally homogeneous medium with Robin-type boundary conditions is used to obtain the Kernel function [known as thermal point spread function (TPSF)] in this inverse problem which can be solved using a conjugate-gradient solution method to determine the unknown initial temperature profile through the depth of the laser-irradiated material. For analysis of IRT signals the 3D Green's function is used to derive the TPSF and a 3D temperature distribution is obtained. The method presented in this paper should provide a useful and computationally rapid means for comparative calculation of 3D temperature distributions in laser irradiated tissue.

2 Theory of Laser Heating

The situation being modeled is shown in Figure 1. The medium, of thickness d, lies parallel to the xy plane. The whole medium is assumed to have the same thermal properties which are independent of temperature. The laser beam of wavelength λ is incident along the positive z direction and is focused over a finite region of the medium. It is assumed to consist of plane waves and to have constant radius over the region of focus. Light energy is absorbed within an arbitrarily shaped absorbing region causing a rise in the temperature of the medium. The temperature, $T(\mathbf{r},t)$, at position $\mathbf{r}$, with coordinates (x,y,z), and time t is given by the 3D linear heat conduction equation[5]

Address all correspondence to C. David Wright; electronic mail: david.wright@exeter.ac.uk

1083-3668/2001/$15.00 © 2001 SPIE

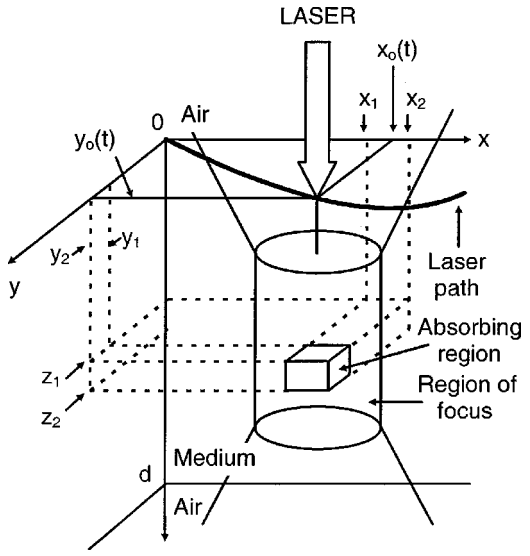

Fig. 1 Schematic illustration of the laser heating situation being modeled. Optical power is absorbed by absorbing regions lying within the region of focus of the scanning laser beam.

$$\rho C \partial T(\mathbf{r},t)/\partial t = K\nabla^2 T(\mathbf{r},t) + S(\mathbf{r},t), \tag{1}$$

where ρ, C, and K are the density, specific heat, and thermal conductivity of the medium material, respectively, and $S(\mathbf{r},t)$ is a heat source term. The solution of Eq. (1) will depend on the initial and boundary conditions imposed. The method used here is a generalization of the approach examined in Refs. 6–8 using appropriate Green's functions. In situations where boundary heat losses can be modeled by the inclusion of the boundary conditions in the Green's function the temperature distribution can be evaluated using the general solution to Eq. (1) which gives the temperature change due to absorption of energy from the laser source as

$$T(\mathbf{r},t) = \frac{1}{\rho C}\int_0^t \int_{V'_{xyz}} G(\mathbf{r},t|\mathbf{r}',t')S(\mathbf{r}',t')dV'dt', \tag{2}$$

where V'_{xyz} is the volume of the region of interest and $G(\mathbf{r},t|\mathbf{r}',t')$ is the medium Green's function. For heat conduction problems the Green's function can be written as[5]

$$G(\mathbf{r},t|\mathbf{r}',t') = G_{xy}(\mathbf{s},t|\mathbf{s}',t')G_z(z,t|z',t'), \tag{3}$$

where $\mathbf{s}$ is the position vector of the point (x,y).

An arbitrarily shaped light-absorbing region can be approximated by a number N_{abs} of finite-sized, rectangular parallelepiped regions defined by the limits $[x_{1(n)},x_{2(n)}]$, $[y_{1(n)},y_{2(n)}]$, and $[z_{1(n)},z_{2(n)}]$, (for n from 1 to N_{abs}) in the x, y, and z directions respectively. The different light-absorbing regions may have different optical properties. The source term in Eq. (1) is the laser energy transformed into heat energy within light-absorbing regions of the medium. For laser heating the source term is assumed to be of the form

$$S(\mathbf{r},t) = S_{\text{laser}}(\mathbf{s},t)S_{\text{absorb}(n)}(z)p(t) - \rho C\omega_p T(\mathbf{r},t), \tag{4}$$

where $S_{\text{laser}}(\mathbf{s},t)$ is the laser power density, $S_{\text{absorb}(n)}(z)$ is the heat generating rate for the nth light-absorbing region, $p(t)$ is the laser intensity modulation, and ω_p is a rate constant. The first part of Eq. (4) models the heat source provided by the laser beam and the second part is a distributed heat loss term. In medical applications[1,18,19] this latter term may be used to model heat loss by uniform perfusion of a liquid (usually blood) through laser-heated tissue.

The temperature distribution produced by the nth light-absorbing region can be written as

$$T(\mathbf{r},t) = \frac{1}{\rho C}\int_{t-\min\{t,T_p\}}^{t} p(t-\tau)Q(\tau) \times I_n(z,\tau)M_n(x,y,t,\tau)d\tau, \tag{5}$$

where T_p is the laser pulse duration, τ is $t-t'$,

$$Q(\tau) = \exp(-\omega_p\tau), \tag{6}$$

$$I_n(z,\tau) = \int_{z_1(n)}^{z_{2(n)}} G_z(z,t|z',t')S_{\text{absorb}(n)}(z')dz', \tag{7}$$

$$M_n(x,y,t,\tau) = \int_{x_{1(n)}}^{x_{2(n)}}\int_{y_{1(n)}}^{y_{2(n)}} G_{xy}(\mathbf{s},t|\mathbf{s}',t') \times S_{\text{laser}}(\mathbf{s}',t')dx'\,dy'. \tag{8}$$

The xy dependence of the Green's function is given by[5]

$$G_{xy}(\mathbf{s},t|\mathbf{s}',t') = \frac{1}{4\pi\mu\tau}\exp\left\{-\left[\frac{(x-x')^2+(y-y')^2}{4\mu\tau}\right]\right\}, \tag{9}$$

where μ is the medium diffusivity $(K/\rho C)$.

The mathematical details of the approach used to determine the temperature distribution throughout the heated region are given in the Appendix. In Appendix 1 the laser power density profile is assumed to be Gaussian with, for completeness, arbitrary time-dependent deflections x_0 and y_0 in the x and y directions, respectively (to allow for the modeling of a moving laser beam if required). Analytic solution of x' and y' integrations in Eq. (8) gives the expression for $M_n(x,y,t,\tau)$ in Eq. (A 1.2). Analytic solution of Eq. (8) for the top-hat laser profile, commonly used in clinical applications, is generally not possible. However, the case of constant illumination over an infinite radius is soluble and may be used as an approximation to the top-hat case. This is also covered in the Appendix.

As discussed in Sec. 1, expressions for the temperature distributions within semi-infinite media have been examined extensively using the Green's function method. However, the expressions obtained are in general quite complicated.[6,8] In this paper the case of a finite-thickness medium is examined. The Green's function z dependence in this case can be written in the simple form[5]

$$G_z(z,t|z',t') = \sum_{m=0}^{\infty} A_m B_m(z)B_m(z')\exp(-\alpha_m^2\mu\tau), \tag{10}$$

where A_m, $B_m(z)$ and α_m are dependent on the boundary conditions imposed at the top and bottom surfaces of the me-

dium. The simple form of the (z,τ) dependence of $G_z(z,t|z',t')$ means that all solutions of Eq. (7) for the finite-thickness medium can be written in the form

$$I_n(z,\tau)=\sum_{m=0}^{\infty} I_{mn}A_mB_m(z)\exp(-\alpha_m^2\mu\tau), \qquad (11)$$

where I_{mn} is an appropriate function of m given by

$$I_{mn}=\int_{z_{1(n)}}^{z_{2(n)}} B_m(z')S_{\text{absorb}(n)}(z')dz' \qquad (12)$$

and can be solved analytically for many heat generating rate models.[6,8] The solution of Eq. (12) for an exponential heat generation rate is given in Sec. 2 of the Appendix. The infinite summation in Eq. (11) can be truncated to a finite sum as described in Ref. 6.

Since the heat conduction equation of Eq. (1) examined in this paper is linear the total temperature distribution can be obtained by simply summing the temperature distributions produced by each of the individual absorbing regions using the expression given in Sec. 3 of the Appendix. In order to obtain the temperature distributions for some specific cases the time integral in Eq. (A 3.1) is evaluated as described in Ref. 6.

3 Heat Generating Rate Model for the Skin

In models for the heating of biological tissue the term $S(\mathbf{r},t)$ in Eq. (1) is used to represent the source terms in both the transport equation for light propagation and the heat conduction equation. In the heat conduction equation the amount of photon energy absorbed by the tissue[1] is

$$S(\mathbf{r},t)=a\psi(\mathbf{r},t), \qquad (13)$$

where a is a constant and $\psi(\mathbf{r},t)$ is the light fluence-rate distribution (the locally available light intensity within the tissue). The fluence rate depends on the component of the tissue that is absorbing the light (chromophore) and is usually strongly wavelength dependent. The main ultraviolet-absorbing chromophores are proteins and nucleic acids, while water is the primary chromophore in the infrared region. For visible wavelengths proteins and pigments are two of the most important chromophores. In particular, the oxygenated hemoglobin protein in blood has strongly wavelength-dependent absorption peaks in the visible region at approximately 418, 542, and 577 nm while the dark melanin pigment in skin causes intense wideband absorption of visible light,[2,13,20,21] the absorption decreasing with increasing laser wavelength.

If biological tissues were simply light-absorbing media the resulting spatial light distribution could be described by the exponential Lambert–Beer law. This is a reasonable approximation when the primary absorbing chromophore is water. However, tissues are turbid media and photons may be absorbed or scattered by structures within them, with both processes leading to attenuation of the laser beam. Photon scattering does not contribute to the heating of the tissue. The generation of heat is due only to photons that are absorbed in the tissue. The presence of photon scattering means that actual light distributions can be substantially different from those estimated using the Lambert–Beer law. Monte Carlo simulations of photon transport can be used to determine fluence rates in turbid media,[1,22–24] but may require long computer runtimes. Diffusion theory[1,25–27] provides a relatively accurate description of light propagation in absorbing and scattering media and closed-form analytic expressions can be found for the fluence rate in many simple 1D cases. An exponential expression for attenuation of light due to a combination of absorption and scattering provides reasonable agreement with transport theory results within the tissue (away from boundary surfaces) and has often been used as an approximation to the heat generating rate,[28,29] with a suitably chosen effective attenuation coefficient. More complicated fluence rate approximations are available but are not considered here. However, these are often simple combinations of decaying and growing exponentials with suitably chosen parameters,[1,2,20,27,29,30] so that the expressions given in Sec. 2 of the Appendix are also applicable in such cases.

The heating of blood within the skin is now examined for application to PWS removal. PWS are congenital vascular malformations of the dermis and laser treatment is based on selective heat deposition into the ectatic dermal blood vessels to produce irreversible thermal damage to these target vessels while keeping the surrounding connective tissue and the overlying epidermis intact.[13] Selective absorption of green or yellow light by the oxyhemoglobin in the blood leads to relatively selective coagulation of the PWS capillaries.

One approach for modeling PWS skin is to approximate the network of enlarged blood vessels by a finite-thickness layer of blood within the dermis giving a three (or four) layer structure[23,31] consisting of epidermis, dermis, blood plexus (and underlying dermis). In Refs. 32 and 33 a two-layer skin model is used, consisting of epidermal and bloodless dermal layers. In Ref. 32 a single rectangular, blood-filled tube is embedded in the dermis to approximate the presence of a blood vessel while in Ref. 33 a single cylindrical blood vessel is used. In Ref. 34 small dermal blood-carrying capillaries within the dermis are approximated by homogeneously distributing blood in the dermis surrounding the single vessel in the model of Ref. 33. In Refs. 12 and 35 these small capillaries are approximated by using an extra layer of dermal blood above the single vessel in the model of Ref. 33. More realistic Monte Carlo optical models can evaluate the fluence rate for skin containing multiple cylindrical blood vessels[22,24] and even a real PWS tissue morphology obtained by 3D reconstruction of a PWS biopsy.[36]

For the purposes of this paper the medium is assumed to consist of epidermis, dermis, and blood. For light and moderately pigmented skin, for which laser treatment of PWS is suitable, the light-absorbing melanin is mainly concentrated in the region of the epidermal/dermal junction.[13,21,37,38] Consequently, the epidermis is modeled here by two infinite-length, infinite-width, and finite-thickness layers[9] as shown in Figure 2. In the upper epidermal layer there is photon scattering only, giving attenuation of the beam. In the lower epidermal layer there is both photon absorption and scattering, giving both heat generation and beam attenuation. It is noted that for highly pigmented skin there is also a high melanin content in the upper layers of the epidermis and laser treatment for PWS is not recommended.[38]

The dermis consists mainly of connective tissue,[37] which is mostly collagen. For this nonpigmented tissue photon absorp-

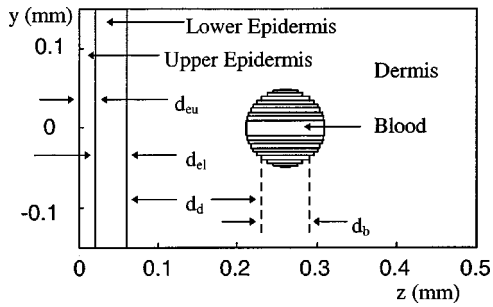

Fig. 2 Schematic illustration of the skin model for the tissue irradiation example under consideration. Light is absorbed in the lower epidermal layer and in 19 light-absorbing blood regions approximating the target blood vessel.

tion is almost negligible for wavelengths greater than 500 nm[32] and it is assumed that no heat is generated within it. However, the beam is attenuated to some extent due to photon scattering by the collagen fibers.[2,13,32] Optical diffusion theory provides a good approximation to transport theory fluence rates for the dermis in the visible wavelength range[25] and adequately describes the variation with time of the surface temperature.[27]

For blood the photon absorption is a more important process than scattering, especially at wavelengths corresponding to the peaks in the oxygenated hemoglobin absorption spectrum mentioned earlier.[2,21] Thus, the Lambert–Beer law can be assumed to apply with the blood absorption coefficient used as the effective attenuation coefficient.[34] In this paper a single cylindrical target blood vessel is approximated by the 19 infinite length (in the x direction), finite-depth (in the z direction) and finite-width (in the y direction) absorbing regions illustrated in Figure 2. In principle multiple blood vessels or a real PWS morphology could be used.

For simplicity, the attenuation of the laser beam in each of the four regions described is assumed to be exponential with appropriately chosen attenuation coefficients, giving

$$P_{\mathrm{att(eu)}}(z') = \exp[-(1-g_{\mathrm{eu}})\gamma_{s(\mathrm{eu})}z']: \quad z' \in (0, d_{\mathrm{eu}}), \tag{14}$$

$$P_{\mathrm{att(el)}}(z' + d_{\mathrm{eu}}) = \exp[-\gamma_{\mathrm{eff(el)}}z']: \quad z' \in (0, d_{\mathrm{el}}), \tag{15}$$

$$P_{\mathrm{att}(d)}(z' + d_{\mathrm{eu}} + d_{\mathrm{el}}) = \exp[-\gamma_{\mathrm{eff}(d)}z']: \quad z' \in (0, d_d), \tag{16}$$

$$P_{\mathrm{att}(b)}(z' + d_{\mathrm{eu}} + d_{\mathrm{el}} + d_d) = \exp[-\gamma_{a(b)}z']: \quad z'(0, d_b), \tag{17}$$

where $P_{\mathrm{att(eu)}}$, $P_{\mathrm{att(el)}}$, $P_{\mathrm{att}(d)}$ and $P_{\mathrm{att}(b)}$ describe the beam attenuation in the upper and lower epidermis, dermis (between the epidermis and the target blood vessel), and blood respectively, $\gamma_{s(\mathrm{eu})}$ is the scattering coefficient for the upper epidermis, g_{eu} is the mean cosine of the scattering angle for the upper epidermis, $\gamma_{\mathrm{eff(el)}}$ is the effective attenuation coefficient for the lower epidermis, $\gamma_{\mathrm{eff}(d)}$ is the effective attenuation coefficient for the dermis, $\gamma_{a(b)}$ is the absorption coefficient for the blood, d_{eu} and d_{el} are the thicknesses of the upper and lower epidermis, respectively, d_d is the distance from the epidermis/dermis boundary to the top of a blood vessel section, and d_b is the thickness of blood in the target blood vessel section as defined in Figure 2. Clearly, the values of d_b and d_d are different for each of the absorbing regions making up the target blood vessel. The value of d_b will lie in the range $(0, d_B)$, where d_B is the diameter of the target blood vessel, giving d_d as $d_0 - d_b/2$, where d_0 is the distance of the center of the target blood vessel below the epidermis/dermis interface. It is noted that the reduced scattering coefficient[2,25] is used as the effective beam attenuation coefficient for the upper epidermis.

For completeness, the attenuation of the laser beam by the dermis below the target blood vessel is given by

$$P_{\mathrm{att}(d)}(z' + d_{\mathrm{eu}} + d_{\mathrm{el}} + d_d + d_b) = \exp[-\gamma_{\mathrm{eff}(d)}z']: \quad z' \in (0, d_D - d_d - d_b), \tag{18}$$

where d_D is the thickness of the dermis. If there is no target vessel in the path of the laser beam the attenuation of the laser beam by the dermis is given by

$$P_{\mathrm{att}(d)}(z' + d_{\mathrm{eu}} + d_{\mathrm{el}}) = \exp[-\gamma_{\mathrm{eff}(d)}z']: \quad z' \in (0, d_D). \tag{19}$$

Attenuation and heat generation in the thin (about 6 μm) blood vessel walls is not included in this simple model.

An effective attenuation coefficient found using optical diffusion theory,[1,26] is given by

$$\gamma_{\mathrm{eff}} = \sqrt{3\gamma_a[\gamma_a + (1-g)\gamma_s]}, \tag{20}$$

where γ_a and γ_s are the absorption and scattering coefficients, respectively, and g is the mean cosine of the scattering angle for the appropriate tissue component. It is noted that γ_a and γ_s are generally very wavelength dependent.

Making use of the attenuation factors defined in Eqs. (14)–(19), the heat generating rates for each of the regions of the medium are

$$S_{\mathrm{absorb(eu)}}(z') = 0: \quad z' \in (0, d_{\mathrm{eu}}), \tag{21}$$

$$S_{\mathrm{absorb(el)}}(z' + d_{\mathrm{eu}}) = EP_{\mathrm{att(eu)}}(d_{\mathrm{eu}})\gamma_{a(\mathrm{el})} \times \exp(-\gamma_{\mathrm{eff(el)}}z'): \quad z' \in (0, d_{\mathrm{el}}), \tag{22}$$

$$S_{\mathrm{absorb}(d)}(z' + d_{\mathrm{eu}} + d_{\mathrm{el}}) = 0: \quad z' \in (0, d_d), \tag{23}$$

$$S_{\mathrm{absorb}(b)}(z' + d_{\mathrm{eu}} + d_{\mathrm{el}} + d_d) = EP_{\mathrm{att(eu)}}(d_{\mathrm{eu}})P_{\mathrm{att(el)}}(d_{\mathrm{el}})P_{\mathrm{att}(d)}(d_d)\gamma_{a(b)} \times \exp(-\gamma_{a(b)}z'): \quad z' \in (0, d_b), \tag{24}$$

where E is the ratio of fluence rate to incident laser irradiance at the tissue surface and $\gamma_{a(\mathrm{el})}$ is the absorption coefficient for the lower epidermis. Equation (23) is used for all regions of the dermis.

Multiple scattering can cause the light fluence rate just below the surface of the tissue to be larger than the incident irradiance.[1,23] The increase in fluence rate relative to the incident irradiance may be about 2–5 with even larger ratios occurring for hollow organs such as blood vessels that act as integrating spheres. Therefore, the value of E may be signifi-

cantly larger than unity, especially for closed cavities. Monte Carlo fluence rate calculations,[12,33] indicate a value for E of about 3 for the case under consideration. Scattering also extends the light fluence rate beyond the lateral dimensions of the incident irradiance. The magnitude of these effects and their importance depends strongly on the scattering and absorbing properties of the tissue and the diameter of the laser spot relative to the penetration depth of the light.

In the model of Figure 2 there is only a single, isolated target blood vessel. In reality there will be many blood vessels present in the dermal layer of the skin. Any blood vessels anterior to the target vessel will cause additional attenuation of the laser beam intended to damage the target, especially if it is deep within the dermis. In Ref. 34 the presence of this dermal blood is modeled by assuming that there is a fraction p of blood homogeneously distributed through the dermis. Linear interpolation between blood and bloodless-dermis optical parameter values is used to give bloody-dermis values. For example, the absorption coefficient for bloody dermis is given as

$$\gamma_{a(bd)} = p\,\gamma_{a(b)} + (1-p)\,\gamma_{a(d)}, \tag{25}$$

where $\gamma_{a(d)}$ is the absorption coefficient for the bloodless dermis. Values for the scattering coefficient and mean cosine of the scattering angle for the bloody dermis are found in the same way and the effective attenuation coefficient for the bloody dermis is then found using Eq. (20). The value of p lies in the range 0–1. ''Normal'' skin has a p value of about 0.01 (i.e., about 1% dermal blood content) while in PWS cases p values are about 0.05–0.1. An alternative approach[12,35] is to represent the dermal blood by an additional thin, attenuating blood layer in the dermis between the epidermis and the target blood vessel.

Having defined the heat-generating rate within the medium it is now necessary to consider the evaluation of the temperature distribution. Defining $T(\mathbf{r},t)$ as the increase in temperature above the ambient skin temperature, $T_{\mathrm{amb(skin)}}$, for an incident laser power of 1 W, then the temperature within the skin for an incident laser power P_0 (in W) is given by

$$T_{\mathrm{skin}}(\mathbf{r},t) = P_0 T(\mathbf{r},t) + T_{\mathrm{amb(skin)}}. \tag{26}$$

Assuming that the skin can be modeled as a thermally homogeneous medium the method outlined in Sec. 2 can be used to obtain the required temperature distribution. The xy dependence of $T(\mathbf{r},t)$ for a Gaussian laser profile and for uniform illumination is given in Sec. 1 of the Appendix.

When there is forced convection of heat from the surfaces of the medium into a steady stream of surrounding fluid (i.e., cooling in a draught) Newton's Law of Cooling states that the rate of heat loss from the body is proportional to the temperature difference between the body and the surrounding fluid. For this case, Robin-type boundary conditions for the temperature at the top and bottom surfaces of the medium apply and are given by

$$\partial T_{\mathrm{skin}}(\mathbf{r},t)/\partial z = H_1(T_{\mathrm{skin}}(\mathbf{r},t) - T_{\mathrm{amb(air)}}): \quad z=0, \tag{27}$$

$$\partial T_{\mathrm{skin}}(\mathbf{r},t)/\partial z = -H_2(T_{\mathrm{skin}}(\mathbf{r},t) - T_{\mathrm{amb(core)}}): \quad z=d, \tag{28}$$

where $T_{\mathrm{amb(air)}}$ and $T_{\mathrm{amb(core)}}$ are the ambient temperatures of the air and body core, respectively, and H_1 and H_2 are convection coefficients for the upper and lower medium/fluid boundaries, respectively. H_1 and H_2 are zero or positive and control the rate of heat flow from the medium surfaces and their values depend on the type of fluid and the flow regime.[39] The boundary condition given by Eq. (27) for a semi-infinite medium has been used elsewhere to examine the effects of surface precooling methods, such as sapphire contact cooling[10] and cryogen spray cooling[9–11] in PWS treatment.

The finite-thickness medium temperature model should give results in agreement with the semi-infinite medium model provided that the medium thickness is chosen to be larger than the maximum distance that heat can diffuse through the layer from its source during the time period under consideration. For the case under consideration this means that the chosen thickness for the dermis in the model should satisfy

$$d_D - d_0 - d_B/2 > L_{\max}, \tag{29}$$

where $L_{\max}$ is the maximum heat diffusion distance in time T_{period}. A reasonable approximation to $L_{\max}$ (Ref. 5) is

$$L_{\max} \approx 4\sqrt{\mu T_{\mathrm{period}}}. \tag{30}$$

For simplicity it is now assumed that the initial air, skin, and core temperatures are equal and set to 30°C. Strictly speaking the surface heat loss should be taken proportional to the temperature difference across the medium interface instead of the temperature difference with respect to the initial skin temperature as implied by Eqs. (27) and (28). However, the simplified assumption should be valid for very short laser pulse durations or for situations where the region outside the heated medium acts as a heat sink.[40] The z-dependent part of the problem can then be solved using the method described in Sec. 2 of the Appendix. The full temperature distribution is then obtained using Eq. (A 3.1) in Sec. 3 of the Appendix.

For situations where the medium cannot be assumed thermally homogeneous, where heat generating rates are more complicated, or where more general boundary conditions are imposed, finite-difference,[28,30,31,41–43] or finite-element methods[44] can be used.

4 Results

In order to apply the model derived in the case of PWS removal it is necessary to use appropriate values for the physical, optical, and thermal parameters of the various skin components. There is much discussion of these in the literature.

Useful information on the location and size of light absorbers within the skin, and estimates of the energy density required to destroy PWS vessels, can be obtained via PPTR[11,14–16] and IRT[17,18] measurements. Temperature profiles through the depth of the skin obtained from PPTR signals clearly distinguish heating of epidermal melanin and PWS blood vessels.[15] A narrow peak is seen in the temperature profile within the epidermis due to melanin absorption.[11,14–16] In Ref. 11 there is a subsurface temperature peak at a depth of approximately 75–80 μm, probably corresponding to the

epidermal/dermal boundary. Computed (1D) epidermis temperature increases derived from these measurements allow for estimation of a limiting laser dose corresponding to the temperature of melanosome explosion.[13] Above this energy density limit there is risk of epidermal injury leading to long term changes of pigmentation and scarring.[15]

Below the epidermal temperature peak the PPTR measurements reveal a broad band of increased temperature values occurring at tissue depths of 100–600 μm.[11,14–16] Hemoglobin distribution within the skin (obtained from microscopic observation of histologic sections of biopsied skin) is in good agreement with this part of the temperature profile,[16] indicating that it is due to heated blood. This broad band of increased temperature values is not due to individual PWS vessels but represents an average temperature increase due to the network of vessels.[11] As heat diffuses to the skin surface, that from PWS vessels and the surrounding dermis will mix to an extent, and the actual rise in temperature of an individual PWS vessel may be much higher than the average temperature values suggested by PPTR results.[14]

Using IRT, 3D temperature distributions within the skin are obtained that clearly show the network of heated PWS blood vessels.[18] The results indicate a depth of 50 μm ($\pm$25 μm) for epidermal melanin[17] and a depth of 150–350 μm[17,18] for PWS blood vessels, in good agreement with PPTR results and values obtained from actual PWS biopsies.[36,41] The IRT images can be used for assessment of the vascular characteristics of proposed treatment sites. Also, since temperatures within individual PWS vessels can be evaluated, it should be possible to optimize the dosimetry for their irreversible destruction.[18]

Taking the results of the studies described above into account, a model for human skin is used here that comprises a two-layer epidermis, a dermis, and an embedded cylindrical blood vessel, as shown in Figure 2. The top epidermis layer is 20 μm thick and is relatively melanin free and nonabsorbing. The lower epidermis layer is 40 μm thick and is assumed to contain the light absorbing melanin. The PWS ''blood vessel'' is assumed to lie at a depth of 200 μm and is 100 μm in diameter.

Typical values for the optical parameters of many types of biological tissue are available,[1,26] including those for the epidermis, dermis, and blood at the wavelengths used in PWS removal.[12,32–34] Thus, absorption and scattering coefficients and angles used in the examples presented here are as shown in Table 1. However, it should be borne in mind that skin properties such as pigmentation, that are different for each individual, will influence the absorption and scattering coefficients.[32]

Thermal conductivity and diffusivity values for many types of biological tissue are also given in Ref. 1. Thermal parameter values for the epidermis, dermis, and blood used in finite difference laser-heating models are given in Refs. 41 and 42. The values for these three components are not too dissimilar, so that the assumption of thermal homogeneity that is used in this paper should be reasonable to a first approximation.

The important laser parameters for PWS removal are the wavelength, spot size, modulation pulse duration, and incident energy density. The wavelength is important because of the absorption characteristics of the various skin components. For the selective targeting of blood vessels it is necessary to use a laser wavelength close to one of the oxy-hemoglobin absorption peaks mentioned earlier. However, the wavelength should also be chosen to reduce the attenuation and absorption of the laser beam by epidermal melanin, so that most of the laser energy reaches the PWS vessels and does not cause excessive heating of (and damage to) the epidermis. Since epidermal melanin absorption decreases with increasing wavelength a long laser wavelength should be used. In particular, values of 577 nm (Ref. 13) and 585 nm,[17,22,35] have been found to be effective,[12,33] and the latter value is used here.

Using Monte Carlo models,[22,36] the energy deposition in the epidermis is estimated to lie in the range of 30–50 J/cm^2 and in blood vessels in the range of 50–350 J/cm^2 for an incident laser irradiation energy density of 1 W/cm^2 (values depend to some extent on laser wavelength).[36] The optimal radiant exposure should cause irreversible damage to the deepest PWS vessels while sparing the overlying epidermis and surrounding dermis. Since the vasculature of any given PWS and the skin pigmentation are patient specific the optimum laser energy density is found to be highly patient dependent. Purpura threshold values lie in the range of 3–4.25 J/cm^2 (Refs. 45 and 46) while values for full treatment generally lie in the range of 6–12 J/cm^2.[9,46] The values of 3.45 and 8 J/cm^2 are used here. The energy density is related to the spot size and pulse duration by Eq. (A 1.7) in Sec. 1 of the Appendix.

Consideration of the penetrating properties of light suggests that the spot diameter should be larger than 3 mm.[12,33] Larger spot size gives greater penetration depth.[12] Thus, the laser spot sizes used are much larger than the dermal distances between PWS blood vessels, which are about 0.1–0.5 mm.[18,36,41–43] Here a spot size of 5 mm is assumed.

The laser pulse duration should be long enough to heat the PWS vessels to temperatures capable of causing irreversible wall damage, but short enough to avoid excessive heating of the epidermis (by direct laser power absorption) and the dermis (by diffusion of heat from the hot blood). The thermal relaxation time for PWS skin is about 1 ms.[12,45] A pulse duration of 0.45 ms is commonly used[46] clinically.

A summary of all relevant parameters used in the simulations is given in Table 1. Using these values in Eqs. (21)–(24) leads to an epidermal energy deposition rate of about 45 W/cm^3 and blood energy deposition rates of about 100–350 W/cm^3 (depending on the vessel diameter, depth, and dermal blood percentage) for an incident laser irradiation energy density of 1 W/cm^2, in good agreement with values obtained from Monte Carlo optical modeling of a real PWS morphology.[36,41] The maximum heat diffusion distance $L_{\max}$ is around 150 μm, as estimated from Eq. (30) (for a time period of about 10 ms). This means that for the finite-thickness medium approximation to be valid the minimum value for the thickness of the dermis is about 400 μm. This is much less than the actual dermis thickness so that the bottom surface cooling coefficient H_2 may, not unreasonably, be set to zero. Initially the top surface cooling coefficient H_1 and the skin perfusion rate ω_p are also set to zero, their effects being analyzed later (see Figure 5).

Figure 3 thus shows the variation of temperature through the medium depth along the beam axis at the end of a 0.5 ms

Table 1 Numerical values for the optical and thermal parameters for the medical laser heating examples.

Model parameter	Value	Model parameter	Value
Pulsed dye laser		Middle layer	47.0 mm^{-1}
Wavelength λ	585 nm	Bottom layer	12.9 mm^{-1}
Beam $1/e$ radius r	2.5 mm, ∞	Embedded cylinder	46.7 mm^{-1}
Scanning speed v	0 m/s	Mean cosine of scattering angle g	
Pulse length T_p	0.5 and 5 ms	Top layer	0.79
Laser energy density E_d	3.45 and 8 J/cm^2	Middle layer	0.79
Medium		Bottom layer	0.79
Material	Human skin	Embedded cylinder	0.995
Top layer	Upper epidermis	Ratio of fluence rate to incident laser irradiance at tissue surface E	3
Middle layer	Lower epidermis	Thermal conductivity K	0.53 $J\,m^{-1}\,s^{-1}°C^{-1}$
Bottom layer	Dermis		
Embedded cylinder	Blood	Specific heat ρC	4.6 $MJ\,m^{-3}°C^{-1}$
Thickness d	0.5 mm	Ambient temperature—air	25°C
Top layer	20 μm	Ambient temperature—skin	30°C
Middle layer	40 μm	Ambient temperature—deep body core	37°C
Bottom layer	0.44 mm	Perfusive losses in the skin	
Embedded cylinder depth	200 μm	Typical perfusion rate for skin ω_p	0.002–0.02 s^{-1}
Embedded cylinder diameter	100 μm	Perfusion rate used for example in text ω_p	100 s^{-1}
Absorption coefficient γ_a		Surface losses to the air	
Top layer	0 mm^{-1}	Typical top surface convection coefficient H_1	100 m^{-1}
Middle layer	1.8 mm^{-1}	Typical top surface evaporation coefficient H_1	2000 m^{-1}
Bottom layer	0.024 mm^{-1}	Top surface cooling coefficient used in text H_1	80 000 m^{-1}
Embedded cylinder	19.1 mm^{-1}	Bottom surface convection coefficient used in text H_2	0
Scattering coefficient γ_s			
Top layer	47.0 mm^{-1}		

pulse for a Gaussian profile laser with incident power density of 6.9 kW/cm^2, giving a laser energy density of 3.45 J/cm^2. The results for a bloodless dermis (i.e., p equal to zero) and various levels of dermal blood are shown. The temperature of the blood in the target vessel rises most significantly. The results for 8% dermal blood match model results for a real PWS morphology well.[42] The occurrence of temperatures greater than 100°C does not necessarily mean that the blood will boil (as mentioned later in Sec. 5). The target vessel blood reaches lower peak temperatures for higher p values as expected. The generation of heat in the target blood vessel and subsequent temperature increase to beyond about 60–70°C should cause irreversible damage to the blood vessel wall and coagulation of the blood, resulting in removal of the abnormal blood vessels. The top surface of the blood vessel reaches the highest temperatures, leading to coagulation and vaporization of the blood.[43] This destruction of the abnormal blood vessels causing PWS eventually results in normal-looking skin. There is only a minor rise in temperature of the epidermis and dermis so that there should be little or no peripheral tissue damage. The epidermal temperature is not affected by the value of p in this simple model.

Figure 4 shows the temperature distribution at the end of the 0.5 ms pulse for a case having 8% dermal blood. The temperature rise is clearly concentrated in the upper region of the blood vessel.[43] For the short pulse used there is very little diffusion of heat out of the light-absorbing regions.

Figure 5 shows the variation of temperature through the medium depth along the beam axis for the case of constant, rather than Gaussian, laser intensity profile. Curve (a) is for a

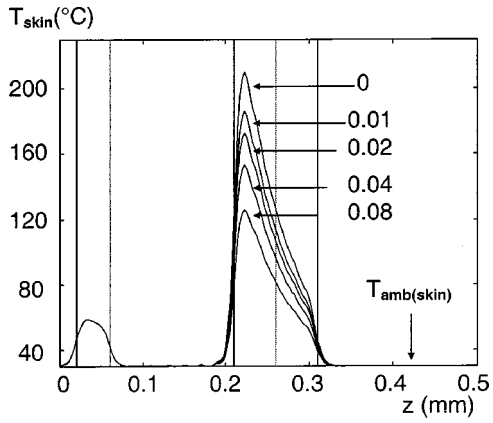

Fig. 3 Temperature vs depth along the beam axis at the end of a 0.5 ms, 3.45 J/cm^2 Gaussian profile laser pulse of 2.5 mm radius for the tissue irradiation example defined in Table 1 and Figure 2 for various values of dermal blood content.

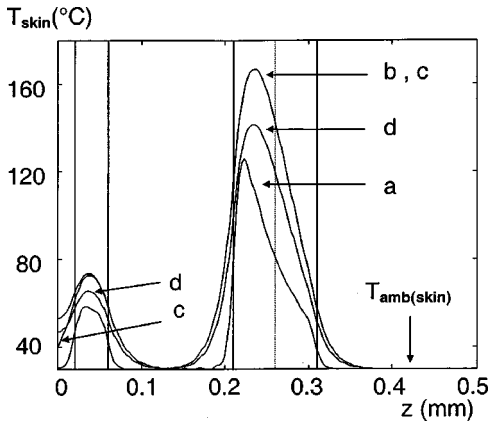

Fig. 5 Temperature vs depth along the beam axis at the end of the laser pulse for constant irradiation using 8% dermal blood content and (a) 0.5 ms pulse with energy density 3.45 J/cm^2; (b) 5 ms pulse with energy density 8 J/cm^2; (c) 5 ms pulse with energy density 8 J/cm^2 with a top surface loss coefficient, H_1, of 80 000 m^{-1}; (d) 5 ms pulse with energy density 8 J/cm^2 with a perfusion rate ω_p of 100 s^{-1}.

laser energy density of 3.45 J/cm^2 and 8% dermal blood content. These results are indistinguishable from those of Figure 3, indicating that the shape of the wide laser profile does not seriously affect the temperature distribution in the vicinity of the blood vessel. Curve (b) of Figure 5 shows the effects of increasing the pulse duration to 5 ms and the incident laser energy density of 8 J/cm^2. When using this longer pulse the heat diffuses further into the dermis. There is also significant heating of the epidermis. Curve (c) of Figure 5 shows the temperature distribution obtained using a surface loss coefficient H_1 equal to 80 000 m^{-1}.[9,10] This large skin/air surface loss term here causes only minor reduction of the temperature in the upper 10 μm of the skin. Clearly, this simulated cooling is not as effective as methods analyzed in Refs. 9–11 and 42 where cryogenic precooling of the skin applied for 20–100 ms before laser heating gave a 10–40°C reduction in temperature over the top 100–200 μm of the skin. It is also apparent from these results that the effects of convection and evaporation, that are modeled by much smaller values[8] for H_1 than that used here (see Table 1), will be negligible for the short heating periods used in PWS applications. Curve (d) of Figure 5 shows the temperature distribution obtained by including skin perfusion rates, i.e., ω_p values, of 100 s^{-1}. Since this value is much larger than actual perfusion rates in tissue,[1] the effect of perfusion over short laser heating periods is also expected to be small.

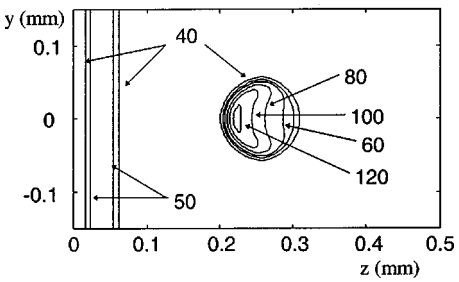

Fig. 4 Temperature contours vs (y, z) for $x=0$ at the end of a 0.5 ms, 3.45 J/cm^2 Gaussian profile laser pulse of 2.5 mm radius for the tissue irradiation example defined in Table 1 and Figure 2 for 8% dermal blood content (i.e., $p=0.08$).

5 Discussion

A simple laser-heating model has been used to derive expressions for temperature distributions within finite-thickness media with simple perfusive and surface losses. The medium may contain any number of light-absorbing parallelepiped regions. These may have different optical properties but, for the time domain approach used here, must have similar thermal properties to the medium in which they lie. For situations in which the absorbing regions have thermal properties which are significantly different from those of the nonabsorbing regions the results are not good[6] and numerical solution techniques, such as the finite difference[28,30,31,41,42] and finite element[44] methods should be used.

The temperature distribution expressions derived are quick and easy to use and produce results that match quite well those of more computationally intensive approaches.[36,41,42] The simple time domain model does however have various limitations resulting from the physical, optical, and thermal simplifications adopted, and these are discussed below.

Physical simplifications include the following assumptions:

- *The interfaces between different layers are all flat and parallel*. On a microscopic scale the air/skin interface is quite rough and therefore it scatters incident radiation.[2,47] Viewed from above, the surface of the skin contains creases forming an approximate triangular grid leading to variations in the skin profile. The peak-to-valley vertical depth of these creases is about 50 μm and the mean horizontal spacing between creases is about 400 μm.[48]
- *The melanin absorber consists of a homogeneous layer within the epidermis*. Melanosomes are however of submicron size and melanocytes are about 25–50 μm in diameter.[13] Thus, the melanin absorbers may be better

modeled as a random distribution of discrete absorbers in the region of the epidermal/dermal interface.

- *The dermis consists a homogeneous structure of connective tissue containing blood vessels*. In fact, the dermis also contains many other structures, including lymph vessels, hair follicles, sweat glands, sebaceous glands, muscles, and nerves,[37] that may affect both its optical and thermal properties.
- *The ectatic blood vessels causing the PWS are simple long, cylinders*. In practice, a complex network of blood vessels is observed.[17,18,36,41–43]

Optical simplifications include the following assumptions:

- *The medium power absorption and heat generating rates can be modeled using exponential functions with attenuation coefficients derived from optical diffusion theory*. It is debatable whether light propagation in biological tissue can be adequately treated by photons whose propagation (including absorption and scattering) is described by transport theory. Diffusion theory results are derived as approximate solutions of the transport equation and since the exponential attenuation of light in tissue is simply an approximation in reasonable agreement with 1D diffusion theory fluence rate results (away from boundary surfaces), the use of Eqs. (14)–(19) and (21)–(24) represents a considerable simplification. At optical and near-infrared wavelengths (0.3–2 μm) there is very intense photon scattering within human tissue[28] so that exponential attenuation may not be an appropriate model. In particular, subsurface maxima are often seen in the fluence rate[1,23] and these are not modeled by a simple decaying exponential. This said, optical diffusion theory does adequately describe the fluence rate in many cases.[27]
- *The optical properties of the epidermis, dermis, and blood are spatially homogeneous*. This may be too restrictive since the structure and pigmentation of tissue show considerable variability. The effects of this variability are examined using a simple optical model.[27]
- *There is blood homogeneously distributed in the dermis*. There may be significant differences in the fluence rate distributions produced for multiple blood vessel configurations and homogeneous dermal blood distributions. However, the homogeneous model with appropriate attenuation parameters can accurately represent discrete blood vessels.[24]

Thermal simplifications include the following assumptions:

- *The skin can be treated as a thermally homogeneous medium*. There may be differences in the thermal properties of the epidermis, dermis, and blood due to their differing chemical and physical components. Different skin component thermal properties can be used in finite difference models for laser heating.[41,42]
- *Surface losses can be modeled by Newton's Law of Cooling*. If there is significant difference in the ambient temperatures of the air, skin, and body core or if there is surface precooling of the skin prior to laser heating more general boundary conditions of the form of Eqs. (27) and (28) are required.[9]

In addition it is pertinent to note the following points:

- Values for the absorption and scattering coefficients γ_a and γ_s measured *in vivo* seem to be much smaller than the values from *in vitro* measurements.[49] Therefore, care must be taken to use suitable values for the optical properties for biological tissue.
- Photocoagulation and dehydration may lead to changes with temperature of both the thermal and optical properties of the tissue and blood.
- The transition of vaporization into boiling, which may cause the temperature to plateau at 100°C,[30] is not considered in the model presented here. The occurrence of a 100°C plateau depends on such factors as the laser beam power density and tissue mechanics and mass transfer properties. The critical vaporization temperature for blood in a laser-heated vessel is not known. A value of 100°C is often assumed since this is the boiling point of water. However, due to superheating effects, tissue temperatures can exceed 100°C prior to vaporization with critical temperatures up to 180°C being reported for laser ablation of aorta.[1]

Clearly, many of the simplifications used to derive the model relate to assumptions of spatial and temporal homogeneity in the physical, optical and thermal properties of the medium. The use of Monte Carlo optical models in conjunction with finite difference thermal models provides a means of simulating more realistic situations.[41,42] However, the time domain method presented here is exceptionally rapid, producing in a matter of seconds on a modest IBM-PC type platform results that match quite well, for the examples presented, those of much more complicated approaches.

6 Conclusions

A time domain method has been used to derive simple expressions for the temperature distributions obtained by laser heating within finite-thickness, thermally homogeneous media with surface losses described by Newton's Law of Cooling. Analytical evaluation of the spatial part of the linear heat conduction problem for an exponential power absorption function leads to a temperature solution that is given as a single integral with respect to time that may be readily and rapidly evaluated using simple numerical integration algorithms. The model has been applied to the heating of blood vessels within the dermis for PWS removal. The temperature distributions obtained are in good agreement with those produced using considerably more computationally intensive Monte Carlo optical and finite difference thermal models. The presence of perfusion and surface losses during laser heating do not appear to produce significant reduction of tissue temperatures.

Acknowledgments

The authors would like to acknowledge the Engineering and Physical Sciences Research Council for supporting this work under Grant Nos. GR/L07734 and GR/M45498.

Appendix

1 The *xy* Dependence of the Temperature Distribution

The laser power density profile is assumed to be Gaussian, with arbitrary deflections x_0 and y_0 in the x and y directions, respectively, giving

$$S_{\text{laser}}(\mathbf{s},t)=\frac{P_0}{\pi r^2}\exp\{-[(x-x_0)^2+(y-y_0)^2]/r^2\}, \tag{A 1.1}$$

where P_0 is the incident laser power and r is the $1/e$ beam radius. Analytic solution of x' and y' integrations[50] in Eq. (8) gives $M_n(x,y,t,\tau)$ for the Gaussian laser profile as

$$\begin{aligned}M_n(x,y,t,\tau)=P_d J(x,y,\tau)K(x,x_0,\tau)&[L(x,x_0,x_{2(n)},\tau)\\&-L(x,x_0,x_{1(n)},\tau)]K(y,y_0,\tau)\\&\times[L(y,y_0,y_{2(n)},\tau)-L(y,y_0,y_{1(n)},\tau)],\end{aligned} \tag{A 1.2}$$

where P_d is the laser power density given by

$$P_d=\frac{P_0}{\pi r^2}, \tag{A 1.3}$$

$$J(x,y,\tau)=r^2\exp[-(x^2+y^2)/(r^2+4\mu\tau)]/(r^2+4\mu\tau), \tag{A 1.4}$$

$$K(\xi,\xi_0,\tau)=\exp[\xi_0(2\xi-\xi_0)/(r^2+4\mu\tau)], \tag{A 1.5}$$

$$L(\xi,\xi_0,\xi_1,\tau)=\frac{1}{2}\operatorname{erfc}\left[\frac{(\xi_1-\xi)r^2+(\xi_1-\xi_0)4\mu\tau}{r\sqrt{4\mu\tau}\sqrt{r^2+4\mu\tau}}\right]. \tag{A 1.6}$$

The incident laser energy density is given by

$$E_d=P_0T_p/(\pi r^2). \tag{A 1.7}$$

The top-hat profile, which produces a uniform illumination over a finite radius R, is given by

$$S_{\text{laser}}(\mathbf{s},t)=\frac{P_0}{\pi R^2}:\ (x-x_0)^2+(y-y_0)^2\leqslant R^2. \tag{A 1.8}$$

Analytic solution of Eq. (8) for this case is generally not possible. However, the solution for uniform illumination over the whole xy plane can be obtained by letting r tend to infinity in the solution for the Gaussian profile to give

$$\begin{aligned}M_n(x,y,t,\tau)=P_d&[E(x,x_{1(n)},\tau)-E(x,x_{2(n)},\tau)]\\&\times[E(y,y_{1(n)},\tau)-E(y,y_{2(n)},\tau)],\end{aligned} \tag{A 1.9}$$

where

$$E(\xi,\xi_1,\tau)=\frac{1}{2}\operatorname{erfc}\left[\frac{\xi_1-\xi}{\sqrt{4\mu\tau}}\right]. \tag{A 1.10}$$

Temperature distributions found using this result will closely approximate those produced by a top-hat profile whose radius is much greater than the extent of the main light-absorbing regions in the xy plane.

2 The *z* Dependence of the Temperature Distribution

When there is forced convection of heat from the surfaces of a medium into a steady stream of surrounding fluid (i.e., cooling in a draught) Newton's Law of Cooling states that the rate of heat loss from the body is proportional to the temperature difference between the body and the surrounding fluid (assumed here to be at an ambient temperature of 0°). For this case the boundary conditions for the temperature at the top and bottom surfaces of the medium are

$$\partial T(\mathbf{r},t)/\partial z=H_1T(\mathbf{r},t):\ z=0, \tag{A 2.1}$$

$$\partial T(\mathbf{r},t)/\partial z=-H_2T(\mathbf{r},t):\ z=d, \tag{A 2.2}$$

where H_1 and H_2 are convection coefficients for the upper and lower medium/fluid boundaries, respectively. H_1 and H_2 are zero or positive and control the rate of heat flow from the medium surfaces and their values depend on the type of fluid and the flow regime.[39]

The Green's function for a finite-thickness medium with surface heat losses given by Eqs. (A 2.1) and (A 2.2) is given by Eq. (10) and the m-dependent factors can be written as[5]

$$A_m=\begin{cases}1/d & :\ m=0,H_1=H_2=0\\ 0 & :\ m=0,H_1+H_2>0\\ \dfrac{2\alpha_m^2}{d(\alpha_m^2+H_1^2)+H_1+H_2\left(\dfrac{\alpha_m^2+H_1^2}{\alpha_m^2+H_2^2}\right)} & :\ m\geqslant 1\end{cases}, \tag{A 2.3}$$

$$B_m(z)=\cos(\alpha_m z)+H_1\sin(\alpha_m z)/\alpha_m. \tag{A 2.4}$$

When both H_1 and H_2 are zero, α_m is given by $m\pi/d$.[5] For cases having nonzero H_1 and/or H_2 values of α_m are found by solving

$$\tan(\alpha_m d)=\alpha_m(H_1+H_2)/(\alpha_m^2-H_1H_2), \tag{A 2.5}$$

which can be rewritten in the form[8]

$$[x^2-(H_1d)(H_2d)]\sin(x)-(H_1+H_2)d\cos(x)=0, \tag{A 2.6}$$

where x is $\alpha_m d$.

A simple heat generating rate model which fits many practical situations quite well is the exponential

$$S_{\text{absorb}(n)}(z) = C_n \exp[-\gamma_n(z - z_{1(n)})], \quad \text{(A 2.7)}$$

where A_n and γ_n are appropriate constants. Using this in Eq. (12) gives[50]

$$I_{mn} = C_n[D(z_{1(n)}) - D(z_{2(n)})\exp(-\gamma_n h_n)]/(\alpha_m^2 + \gamma_n^2), \quad \text{(A 2.8)}$$

where $h_n(=z_{2(n)} - z_{1(n)})$ is the thickness of the nth light-absorbing region and

$$D(z) = (\gamma_n + H_1)\cos(\alpha_m z) - (\alpha_m^2 - \gamma_n H_1)\sin(\alpha_m z)/\alpha_m. \quad \text{(A 2.9)}$$

The simple Lambert–Beer law has C_n equal to γ_n, which is the absorption coefficient for the light-absorbing region.

3 The Final Temperature Distribution

Since the heat conduction equation of Eq. (1) is assumed to be linear the total temperature distribution can be obtained by simply summing the temperature distributions produced by each of the individual absorbing regions giving

$$\begin{aligned} T(\mathbf{r},t) = \frac{P_d}{\rho C} \int_{t-\min\{t,T_p\}}^{t} & p(t-\tau)Q(\tau)J(x,y,\tau) \\ & \times K(x,x_0,\tau)K(y,y_0,\tau) \\ & \times \sum_{n=1}^{N_{\text{abs}}} I_n(z,\tau)[L(x,x_0,x_{2(n)},\tau) \\ & - L(x,x_0,x_{1(n)},\tau)][L(y,y_0,y_{2(n)},\tau) \\ & - L(y,y_0,y_{1(n)},\tau)]d\tau. \end{aligned} \quad \text{(A 3.1)}$$

This can be used to evaluate the temperature distribution within a thermally homogeneous medium containing light-absorbing regions with different optical properties.

References

1. *Optical-Thermal Response of Laser-Irradiated Tissue*, A. J. Welch and M. J. C. Van Gemert, Eds., Plenum, New York (1995).
2. M. H. Niemz, *Laser-Tissue Interactions: Fundamentals and Applications*, Springer, Berlin (1996).
3. *Laser Annealing of Semiconductors*, J. M. Poate and J. W. Mayer, Eds., Academic, New York (1982).
4. A. B. Marchant, *Optical Recording: A Tutorial Overview*, Addison-Wesley, Reading, MA (1990).
5. H. S. Carslaw and J. C. Jaeger, *Conduction of Heat in Solids*, 2nd ed., Clarendon, Oxford (1959).
6. M. K. Loze and C. D. Wright, ''Temperature distributions in semi-infinite and finite-thickness media as a result of absorption of laser light,'' *Appl. Opt.* **36**, 494–507 (1997).
7. P. Loza, D. Kouznetsov, and R. Ortega, ''Temperature distribution in a uniform medium heated by absorption of a Gaussian light beam,'' *Appl. Opt.* **33**, 3831–3836 (1994).
8. M. K. Loze and C. D. Wright, ''Temperature distributions in laser-heated semi-infinite and finite-thickness media with convective surface losses,'' *Appl. Opt.* **37**, 6822–6832 (1998).
9. B. Anvari, B. S. Tanenbaum, T. E. Milner, S. Kimel, L. O. Svaasand, and J. S. Nelson, ''A theoretical study of the thermal response of skin to cryogen spray cooling and pulsed laser irradiation: implications for treatment of Port Wine Stain birthmarks,'' *Phys. Med. Biol.* **40**, 1451–1465 (1995).
10. B. Anvari, T. E. Milner, B. S. Tanenbaum, and J. S. Nelson, ''A comparative study of human skin thermal response to sapphire contact and cryogen spray cooling,'' *IEEE Trans. Biomed. Eng.* **45**, 934–941 (1998).
11. J. H. Torres, J. S. Nelson, B. S. Tanenbaum, T. E. Milner, D. M. Goodman, and B. Anvari, ''Estimation of internal skin temperatures in response to cryogen spray cooling: implications for laser therapy of Port Wine Stains,'' *IEEE J. Sel. Top. Quantum Electron.* **5**, 1058–1066 (1999).
12. M. J. C. Van Gemert, A. J. Welch, J. W. Pickering, and O. T. Tan, ''Laser treatment of Port Wine Stains,'' in *Optical-Thermal Response of Laser-Irradiated Tissue*, A. J. Welch and M. J. C. Van Gemert, Eds., Chap. 23, pp. 789–829, Plenum, New York (1995).
13. R. R. Anderson and J. A. Parrish, ''Selective photothermolysis: Precise microsurgery by selective absorption of pulsed radiation,'' *Science* **220**, 524–527 (1983).
14. S. L. Jacques, J. S. Nelson, W. H. Wright, and T. E. Milner, ''Pulsed photothermal radiometry of Port-Wine Stain lesions,'' *Appl. Opt.* **32**, 2439–2446 (1993).
15. T. E. Milner, D. M. Goodman, B. S. Tanenbaum, and J. S. Nelson, ''Depth profiling of laser-heated chromophores in biological tissues by pulsed photothermal radiometry,'' *J. Opt. Soc. Am. A* **12**, 1479–1488 (1995).
16. T. E. Milner, D. J. Smithies, D. M. Goodman, A. Lau, and J. S. Nelson, ''Depth determination of chromophores in human skin by pulsed photothermal radiometry,'' *Appl. Opt.* **35**, 3379–3385 (1996).
17. M. J. C. Van Gemert et al., ''Non-invasive determination of Port Wine Stain anatomy and physiology for optimal laser treatment strategies,'' *Phys. Med. Biol.* **42**, 937–950 (1997).
18. S. A. Telenkov, B. S. Tanenbaum, D. M. Goodman, J. S. Nelson, and T. E. Milner, ''*In vivo* infrared tomographic imaging of laser-heated blood vessels,'' *IEEE J. Sel. Top. Quantum Electron.* **5**, 1193–1199 (1999).
19. A. J. Welch, E. H. Wissler, and L. A. Priebe, ''Significance of blood flow in calculations of temperature in laser irradiated tissues,'' *IEEE Trans. Biomed. Eng.* **27**, 164–166 (1980).
20. R. R. Anderson, J. Hu, and J. A. Parrish, ''Optical radiation transfer in the human skin and application in *in vivo* remittance spectroscopy,'' in *Bioengineering and the Skin*, R. Marks and P. A. Payne, Eds., Chap. 28, pp. 253–265, MTP, Lancaster (1981).
21. J. W. Feather, J. B. Dawson, D. J. Barker, and J. A. Cotterill, ''A theoretical and experimental study of the optical properties of *in vivo* skin,'' in *Bioengineering and the Skin*, R. Marks and P. A. Payne, Eds., Chap. 30, pp. 275–281, MTP, Lancaster (1981).
22. G. W. Lucassen, W. Verkruysse, M. Keijzer, and M. J. C. Van Gemert, ''Light distributions in a Port Wine Stain model containing multiple cylindrical and curved blood vessels,'' *Lasers Surg. Med.* **18**, 345–357 (1996).
23. A. J. Welch and M. Gardner, ''Monte Carlo model for determination of the role of heat generation in laser-irradiated tissue,'' *Trans. ASME, J. Biomech. Eng.* **119**, 489–495 (1997).
24. W. Verkruysse, G. W. Lucassen, F. De Boer, D. J. Smithies, J. S. Nelson, and M. J. C. Van Gemert, ''Modelling light distributions of homogeneous versus discrete absorbers in light irradiated turbid media,'' *Phys. Med. Biol.* **42**, 51–65 (1997).
25. M. J. C. Van Gemert, S. L. Jacques, H. J. C. M. Sterenborg, and W. M. Star, ''Skin optics,'' *IEEE Trans. Biomed. Eng.* **36**, 1146–1154 (1989).
26. W. F. Cheong, S. A. Prahl, and A. J. Welch, ''A review of the optical properties of biological tissues,'' *IEEE J. Quantum Electron.* **26**, 2166–2185 (1990).
27. I. A. Vitkin, B. C. Wilson, and R. R. Anderson, ''Analysis of layered scattering materials by pulsed photothermal radiometry: application to photon propagation in tissue,'' *Appl. Opt.* **34**, 2973–2982 (1995).
28. A. J. Welch, ''The thermal response of laser irradiated tissue,'' *IEEE J. Quantum Electron.* **20**, 1471–1481 (1984).
29. D. Decker-Dunn, D. A. Christensen, W. Mackie, J. Fox, and G. M. Vincent, ''Optothermal mathematical model and experimental studies for laser irradiation of arteries in the presence of blood flow,'' *Appl. Opt.* **28**, 2263–2272 (1989).
30. J. H. Torres, M. Motamedi, J. A. Pearce, and A. J. Welch, ''Experimental evaluation of mathematical models for predicting the thermal response of tissue to laser irradiation,'' *Appl. Opt.* **32**, 597–606 (1993).
31. M. J. C. Van Gemert, W. J. A. De Kleijn, and J. P. Hulsbergen-Henning, ''Temperature behaviour of a model Port-Wine Stain during argon laser coagulation,'' *Phys. Med. Biol.* **27**, 1089–1104 (1982).
32. C. T. W. Lahaye and M. J. C. Van Gemert, ''Optimal laser param-

eters for Port Wine Stain therapy: a theoretical approach,'' *Phys. Med. Biol.* **30**, 573–587 (1985).
33. M. J. C. Van Gemert, J. W. Pickering, and A. J. Welch, ''Modeling laser treatment of Port-Wine Stains,'' in *Management and Treatment of Benign Cutaneous Vascular Lesions*, O. T. Tan, Ed., Chap. 2, pp. 24–47, Lea and Febiger, Philadelphia, PA (1992).
34. W. Verkruysse, J. W. Pickering, J. F. Beck, M. Keijzer, and M. J. C. Van Gemert, ''Modeling the effect of wavelength on pulsed dye laser treatment of Port Wine Stains,'' *Appl. Opt.* **32**, 393–398 (1993).
35. M. J. C. Van Gemert, A. J. Welch, J. W. Pickering, O. T. Tan, and G. H. M. Gijsbers, ''Wavelengths for laser treatment of Port Wine Stains and Telangiectasia,'' *Lasers Surg. Med.* **16**, 147–155 (1995).
36. J. K. Barton, T. J. Pfefer, A. J. Welch, D. J. Smithies, J. S. Nelson, and M. J. C. Van-Gemert, ''Optical Monte Carlo modeling of a true Port Wine Stain anatomy,'' *Opt. Express* **2**, 391–396 (1998). Document Number 4311 from: http://epubs.osa.org/opticsexpress
37. J. H. Epstein, ''Photomedicine,'' in *The Science of Photobiology*, K. C. Smith, Ed., Chap. 7, pp. 175–207, Plenum, New York (1977).
38. A. K. Kurban, ''Evaluation, diagnosis and selection of patients for laser and nonlaser treatment,'' in *Management and Treatment of Benign Cutaneous Vascular Lesions*, O. T. Tan, Ed., Chap. 3, pp. 48–52, Lea and Febiger, Philadelphia, PA (1992).
39. A. Bejan, *Heat Transfer*, Wiley, New York (1993).
40. B. J. Bartholomeusz, ''Thermomagnetic marking of rare-earth-transiton-metal thin films,'' *J. Appl. Phys.* **65**, 252–258 (1989).
41. T. J. Pfefer, J. K. Barton, D. J. Smithies, T. E. Milner, J. S. Nelson, M. J. C. Van Gemert, and A. J. Welch, ''Modeling laser treatment of Port Wine Stains with a computer-reconstructed biopsy,'' *Lasers Surg. Med.* **24**, 151–166 (1999).
42. T. J. Pfefer, D. J. Smithies, T. E. Milner, M. J. C. Van-Gemert, J. S. Nelson, and A. J. Welch, ''Bioheat transfer analysis of cryogen spray cooling during laser treatment of port wine stains,'' *Lasers Surg. Med.* **26**, 145–157 (2000).
43. J. K. Barton, D. X. Hammer, T. J. Pfefer, D. J. Lund, B. E. Stuck, and A. J. Welch, ''Simultaneous irradiation and imaging of blood vessels during pulsed laser delivery,'' *Lasers Surg. Med.* **24**, 236–243 (1999).
44. R. Splinter, S. Y. Semenov, G. A. Nanney, L. Littmann, J. R. Tuntelder, R. H. Svenson, C. H. Chuang, and G. P. Tatsis, ''Myocardial temperature distribution under CW Nd:YAG laser irradiation in *in vitro* and *in vivo* situations: Theory and experiment,'' *Appl. Opt.* **34**, 391–399 (1995).
45. C. C. Dierickx, J. M. Casparian, V. Venugopalan, W. A. Fairinelli, and R. R. Anderson, ''Thermal relaxation of Port-Wine Stain vessels probed *in vivo*: The need for 1–10 millisecond laser pulse treatment,'' *J. Invest. Dermatol.* **105**, 709–714 (1995).
46. J. M. Garden, L. L. Polla, and O. T. Tan, ''The treatment of Port-Wine Stains by the pulsed dye laser,'' *Arch. Dermatol.* **124**, 889–896 (1988).
47. O. T. Tan, ''Pulsed dye laser treatment of adult Port-Wine Stains,'' in *Management and Treatment of Benign Cutaneous Vascular Lesions*, O. T. Tan, Ed., Chap. 6, pp. 83–99, Lea and Febiger, Philadelphia, PA (1992).
48. J. Ferguson and J. C. Barbanel, ''Skin surface patterns and the directional mechanical properties of the dermis,'' in *Bioengineering and the Skin*, R. Marks and P. A. Payne, Eds., Chap. 10, pp. 83–92, MTP, Lancaster (1981).
49. R. Graaff, A. C. M. Dassel, M. H. Koelink, F. F. M. De Mul, J. G. Aarnoudse, and W. G. Zijlstra, ''Optical properties of human dermis *in vitro* and *in vivo*,'' *Appl. Opt.* **32**, 435–447 (1993).
50. I. S. Gradsteyn and I. M. Ryzhik, *Tables of Integrals, Series and Products*, Academic, New York (1965).